ANALYSIS OF STRAIN DEPENDENT DAMPING IN METALS VIA MODELING OF MATERIAL POINT HYSTERESIS

by

Edward J. Graesser* and Catherine R. Wong

David Taylor Research Center
Ship Materials Engineering Department
Bethesda, Maryland, 20084-5000

ABSTRACT

In strain dependent (or nonlinear) high damping metals, measured values of damping vs. strain are often inconsistent for different damping test configurations. To better understand the nature of such inconsistencies shear and bending test configurations were modeled analytically. A hysteretic material point stress-strain relationship was used for each modeling configuration. This model is similar to established constitutive laws of viscoplastic behavior and has been adapted especially for the study of nonlinear hysteresis and the problem of strain dependent damping. Analytical material response analyses of bending and torsion samples indicated that when the damping of a single nonlinear material is plotted against the one-dimensional local strain of the sample, highly discrepant results are produced. However, when the same results are plotted against an invariant measure of three-dimensional local distortion the agreement improves considerably. The method can also be applied to homogeneous isotropic nonlinear damping materials that are not metallic (such as amorphous nonlinear high damping polymers).

* Presenting Author, ONT/ASEE Postdoctoral Fellow, Business Telephone: (301) 267-2835

INTRODUCTION

In addition to add-on damping techniques currently being used in the Navy, material damping is being investigated as a potential means of further reducing machine vibration, noise, and sound emission in seafaring vessels. Ideally a high damping structural material provides a sufficient amount of both stiffness and damping so as to be used as a sole machine part or vibrating element without added treatments. Such materials are most useful for oscillating parts or elements that cannot be damped by conventional external treatments. Also these materials can be useful in situations where heat or other environmental factors (e.g. moisture, corrosion) have to be considered. This approach is also useful in damping longitudinal vibrations which cannot be effectively controlled by external treatments.

Because high stiffness and strength are required in many important applications, metals which possess a large inherent damping capacity have been extensively sought [1,2]. Some specific applications include gears and gear webs, pump castings, engine parts, propellers, and others (see [1]). High damping metals are also used as plug inserts and cladding, and such applications can provide a reduction of resonant amplification factors as well as the attenuation of ringing [1].

Generally "high damping" in metal is a measured peak loss factor or phase lag with a value of 10^{-2} or higher. Indeed many alloy compositions have been studied and found to possess such levels of damping (e.g. see [3-8]). Mechanisms that give rise to damping in metals include: movement of point defects, dislocations, or domain walls. These effects give rise to macroscopic hysteresis and thus damping. For example, in Cu-Mn high damping alloys straining the material induces movement of twin boundaries in the antiferromagnetic matrix, even at low strain levels (10^{-6} to 10^{-4}) [3]. High damping metals possess strain dependent characteristics because the primary damping mechanisms function over a finite range of strain. For example, in magnetostrictive materials a minimum strain is necessary to move magnetic domain boundaries away from their pinning points and thus activate the damping mechanism. However, once a maximum strain is reached which produces full alignment of the magnetic domains the boundaries are no longer able to move and the primary damping mechanism is saturated. Such effects are apparent by virtue of a well defined peak in the plot of measured damping vs. specimen strain. Examples of magnetostrictive metallic materials exhibiting strain-dependent damping are given in Fig. 1. Because the measured damping data varies with changes in specimen strain amplitude the character of this type of response is called nonlinear. A generalized stress-strain diagram corresponding to such nonlinear damping mechanisms is illustrated in Fig. 2. Note from this figure that the response that is hysteretic with a damping mechanism that becomes saturated at a strain of ε_0.

The data obtained for a single strain dependent material in different test configurations is often inconsistent. Data from separate bending and torsion tests [3] given in Fig. 3 shows this effect; indeed the results indicate that the torsional tests produce significantly higher values of damping for common levels of peak sample strain. However it is important to note that the strains on the abscissa are shear strains in the case of torsional data and axial strains in the case of bending data. These separate strains are not equivalent and the consequence of plotting damping data vs strain in this manner will be discussed in the analysis section of this paper.

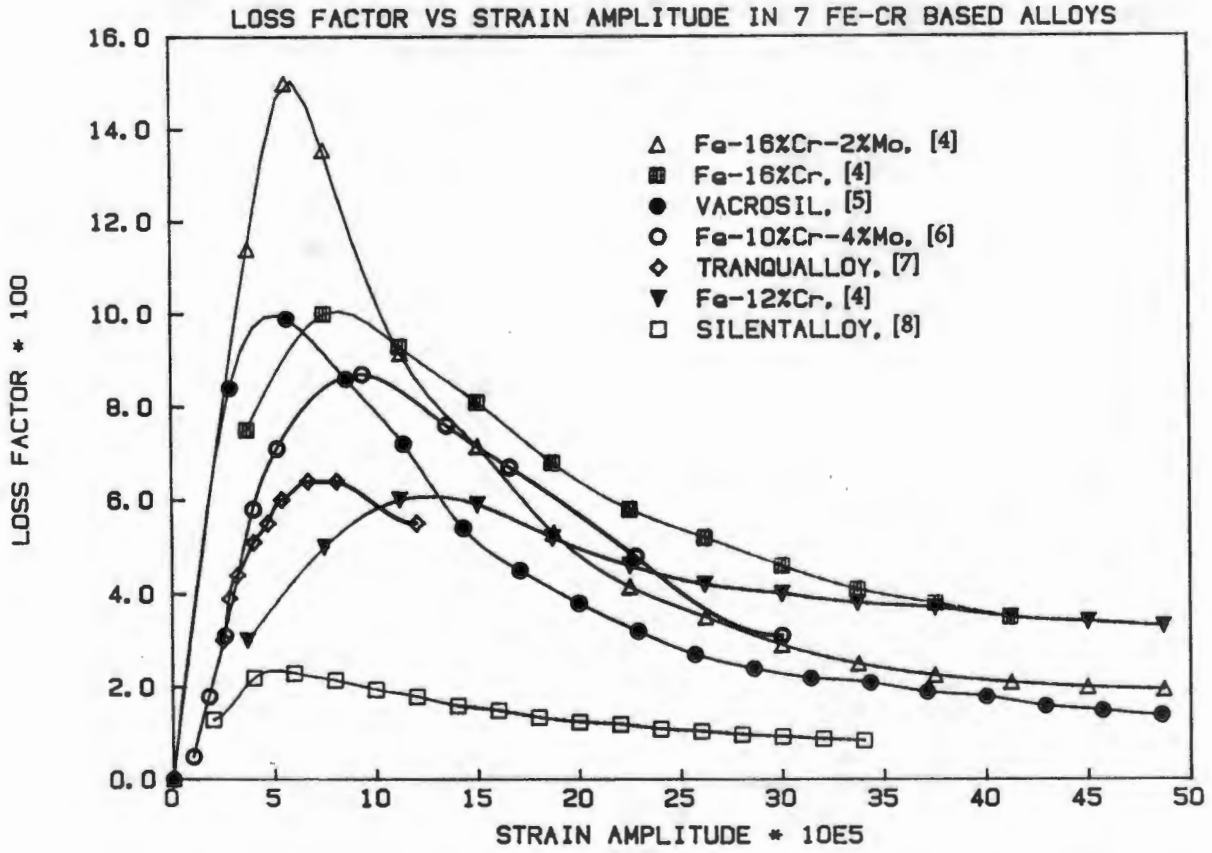

Figure 1: Strain Amplitude Dependent Damping in Fe-Cr Based High Damping Alloys

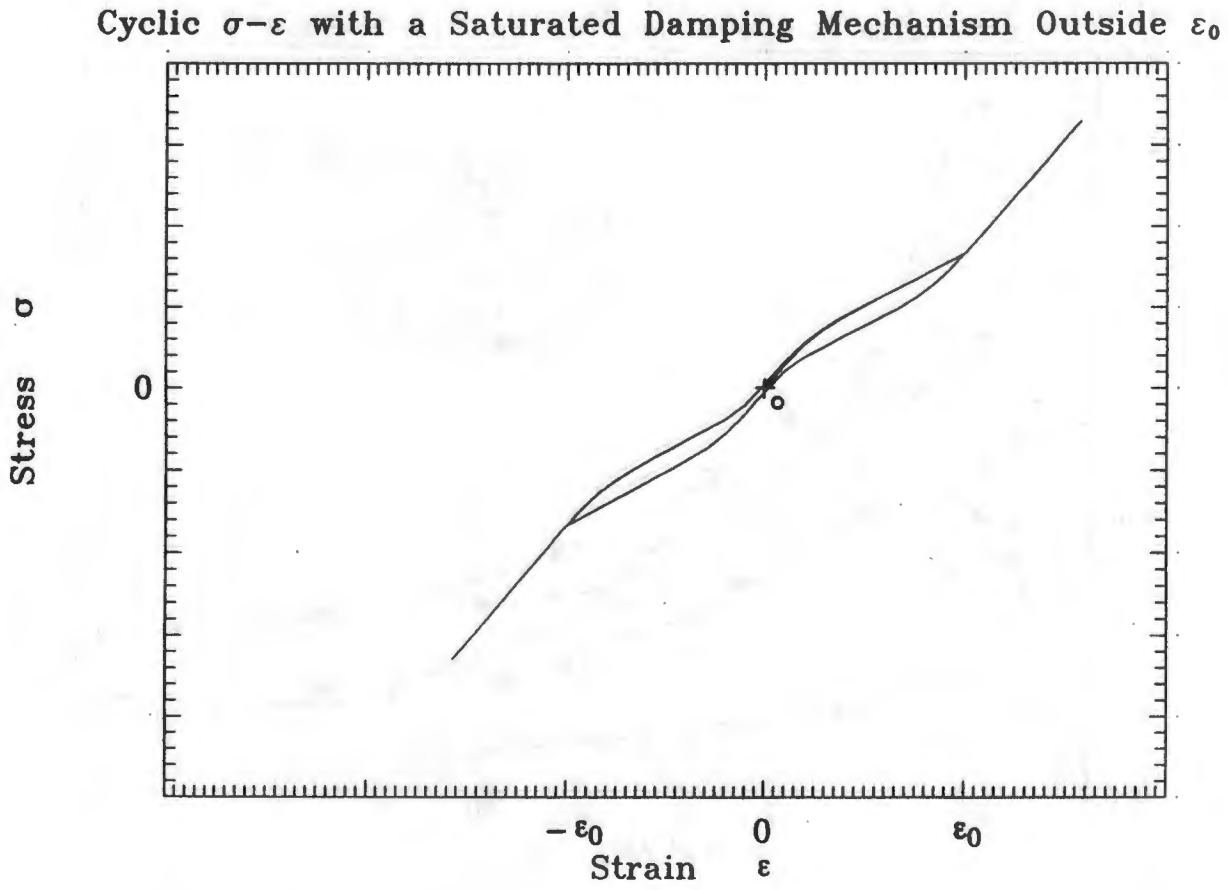

Figure 2: Generalized Macroscopic Hysteresis of Nonlinear Damping Materials

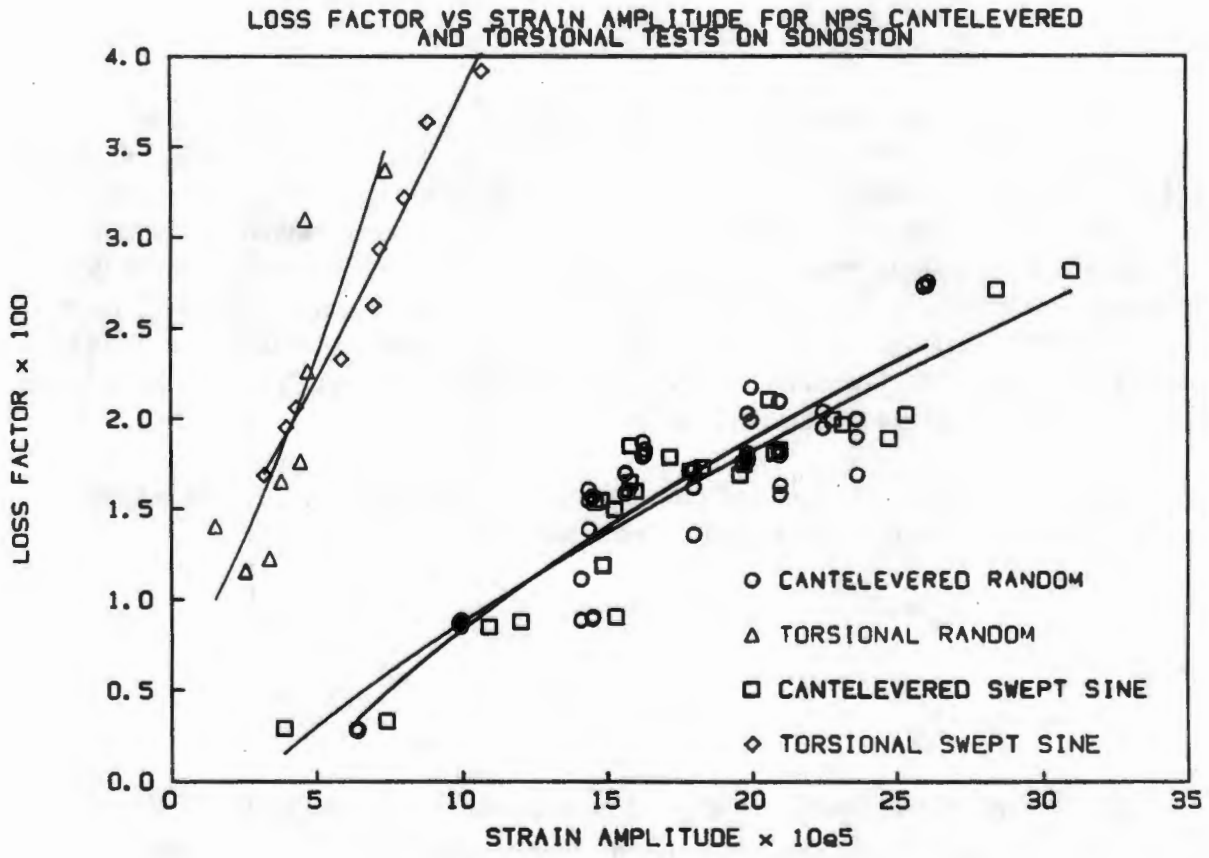

Figure 3: Strain Dependent Damping of Cu-Mn in Separate Bending and Torsion Tests [3]

Strain dependent materials are, at best, difficult to model analytically because of their nonlinear characteristics. Early work in this area concentrated on evaluating the damping of members by combining material energy absorbing properties with geometric and stress distribution factors [9,10]. Another approach is to use a constitutive law which describes nonlinear material behavior and hysteresis at a point, and this approach will be used here. Many such laws exist (e.g. see [11,12]), but these are usually specific to postyielding viscoplastic behavior and large strain levels. In this paper a proposed constitutive law [13] for the stress-strain behavior of shape memory alloys is adapted to the case of nonlinear damping. The equations of this law were applied to the cases of simple uniaxial tension-compression and shear loading, and then were expanded to analyze beam and shaft test samples in bending and torsion respectively. The strain dependent nature of each test configuration was computed, and because this behavior was of primary interest, temperature and frequency effects were not considered.

ANALYSIS

In order to make a useful study of strain dependent damping, a three-dimensional constitutive law of hysteretic material behavior was used in analyses. The law, which is of the viscoplastic type, was originally developed to model the large strain hysteretic behavior of shape memory alloys [13], and especially superelastic behavior. This choice of modeling schemes was pursued because the hysteretic response of superelastic materials is similar in character to that high damping metals (see Fig. 2), except that the stress and strain levels are different by many orders of magnitude. This does not prevent the use of the constitutive law, however, as long as the material properties of the law can be scaled to accommodate the lower stress and strain levels associated with the dissipative mechanisms in the damping material.

The constitutive law is for homogeneous and isotropic material behavior and is based upon a separation of strain and strain rate into elastic and inelastic components:

$$\varepsilon_{ij} = \varepsilon_{ij}^{el} + \varepsilon_{ij}^{in} \tag{1a}$$

$$\dot{\varepsilon}_{ij} = \dot{\varepsilon}_{ij}^{el} + \dot{\varepsilon}_{ij}^{in} \tag{1b}$$

Here an overhead dot represents ordinary time differentiation. Thus ε_{ij} and $\dot{\varepsilon}_{ij}$ are the three-dimensional tensors of strain and strain rate, and the superscripts "el" and "in" designate the respective elastic and inelastic components of each. The elastic component follows directly from the theory of elasticity [14]:

$$\varepsilon_{ij}^{el} = \frac{1+\nu}{E}\sigma_{ij} - \frac{\nu}{E}\sigma_{kk}\,\delta_{ij} \tag{2}$$

where σ_{ij} is the stress tensor, δ_{ij} is the Kronecker delta,[1] and where E and ν are the elastic material constants.

---

[1] $\delta_{ij}=1$ if $i=j$, $\delta_{ij}=0$ if $i\neq j$, $i,j=1,2,3$

The basic equations for the evolution of inelastic strain were taken from a model of shape memory alloy behavior [13]. In this model the growth of inelastic strain is a function of backstress β_{ij}, which is a variable that accounts for internal stress fields in the material. In order to model the saturation of damping mechanisms a unit step function was included to stop the growth of inelastic strain after a limiting value of distortion. This resulted in the following set of equations:

$$\dot{\varepsilon}_{ij}^{in} = \sqrt[+]{3K_2}\left[\sqrt[+]{3J_2}\right]^{n-1}\left[\frac{s_{ij}-b_{ij}}{Y}\right]\left\{u\left[\sqrt{3I_{2_0}}-\sqrt[+]{3I_2}\right]\right\} \tag{3}$$

$$b_{ij} = \frac{2}{3}E\alpha\left[\varepsilon_{ij}^{in} + f_T\frac{e_{ij}}{\frac{2}{3}\sqrt[+]{3I_2}}\,\mathrm{erf}\left[\frac{2}{3}a\sqrt[+]{3I_2}\right]\left\{u\left[-\dot{I}_2\right]\right\}\right] \tag{4}$$

where e_{ij}, s_{ij}, and b_{ij} are the deviatoric tensors of strain, stress and backstress respectively; the difference $s_{ij} - b_{ij}$ is often referred to as the effective stress. The quantities I_2, J_2, and K_2 are the second order invariants of the deviatoric tensors of strain, dimensionless effective stress, and strain rate, respectively. All these quantities are formally described below:

$$e_{ij} = \varepsilon_{ij} - \frac{1}{3}\varepsilon_{kk}\delta_{ij} \quad , \qquad I_2 = \frac{1}{2}e_{ij}e_{ij} \quad , \qquad K_2 = \frac{1}{2}\dot{e}_{ij}\dot{e}_{ij}$$

$$s_{ij} = \sigma_{ij} - \frac{1}{3}\sigma_{kk}\delta_{ij}$$

$$b_{ij} = \beta_{ij} - \frac{1}{3}\beta_{kk}\delta_{ij} \quad , \qquad J_2 = \frac{1}{2}\frac{s_{ij}-b_{ij}}{Y}\frac{s_{ij}-b_{ij}}{Y}$$

Thus the growth of inelastic strain is a function of stress, backstress, and strain rate. Note that plus sign appearing with the radical sign of the square root of the invariants in Eqs. (3)-(4) indicates that the square root, once taken, is to be positive (i.e. the absolute value of the square root). Also, I_2 represents a measure of volumetric distortion that is invariant with respect to coordinate transformations, and this will be an important quantity in the forthcoming discussion.

To summarize, the material constants in Eqs. (2)-(4) are:

- E: Axial elastic modulus
- ν: Poisson ratio of elastic material
- Y: Axial stress level where the damping mechanism is activated thus giving rise to an inelastic response[2]
- α: Constant determining the slope of the inelastic region = $E_y/(E - E_y)$, where E_y is the inelastic slope

[2] The material constant Y, as it is used here, corresponds to a stress whereupon the slope of the axial stress-strain curve is lowered to accomodate the activation of internal damping mechanisms. Therefore Y represents a material constant that is analogous to the yield stress of large strain plastic behavior (indeed for the constitutive law in [11] Y does represent the yield stress) and above this stress the inelastic response is important.

n: Constant controlling the sharpness of transition from elastic to inelastic behavior

f_T: Constant controlling the size of the hysteresis loop

a: Constant controlling the amount of elastic recovery during unloading

Also, Eqs. (3) and (4) contain two special functions: the error function, erf( ), and the unit step function, {u( )}. Simply stated the purpose of the error and unit step functions contained in Eq. (4) is to allow for the recovery of accumulated inelastic strain during unloading, and thus simulate the unique behavior of superelastic materials [13]. As stated earlier the consequence of the unit step function in Eq. (3) is to eliminate inelastic growth outside a limiting value of volumetric distortion.

Let us take a moment to explain the role of the inelastic response in the modeling of strain dependent damping. The inelastic component of strain is responsible for the dissipation of energy that takes place in cyclic loading. Equations (1)-(4) have been used to represent the macroscopic stress-strain behavior of shape memory alloys, and especially superelastic materials [13]. The hysteretic character of superelasticity is macroscopically similar to that of nonlinear anelasticity except that the respective stress and strain levels of each type of response are different by many orders of magnitude. Therefore, the inelastic response governed by Eqs. (3)-(4) can be used to macroscopically represent the effect of a nonlinear anelastic damping mechanism.

By using Eqs. (1)-(4), a number of special cases can be considered. First let us consider the cases of uniaxial tension-compression and pure shear loading. The state of uniaxial loading (superscript u) is described by:

$$\varepsilon_{ij}^{u} = \begin{bmatrix} \varepsilon & 0 & 0 \\ 0 & -\mu\varepsilon & 0 \\ 0 & 0 & -\mu\varepsilon \end{bmatrix} \qquad \dot{\varepsilon}_{ij}^{u} = \begin{bmatrix} \dot{\varepsilon} & 0 & 0 \\ 0 & -\rho\dot{\varepsilon} & 0 \\ 0 & 0 & -\rho\dot{\varepsilon} \end{bmatrix} \qquad \sigma_{ij}^{u} = \begin{bmatrix} \sigma & 0 & 0 \\ 0 & 0 & 0 \\ 0 & 0 & 0 \end{bmatrix} \qquad \beta_{ij}^{u} = \begin{bmatrix} \beta & 0 & 0 \\ 0 & 0 & 0 \\ 0 & 0 & 0 \end{bmatrix}$$

Here ε, σ, and β are the axial strain, stress, and backstress in the x direction of Cartesian space, respectively. Also the lateral strain and strain rate induced by the Poisson effect ($-\mu\varepsilon$ and $-\rho\dot{\varepsilon}$) are associated with the coefficients μ and ρ respectively. Because of the nonlinear effect induced by the damping mechanism μ and ρ are neither constant nor equal. In order to evaluate these factors the lateral strain and strain rate are decomposed into elastic and inelastic parts. The total lateral strain is decomposed in the same way. The elastic component is related to the elastic axial strain by the elastic Poisson ratio ν, and the inelastic component is related to the axial inelastic response in an incompressible manner (recall that the Poisson ratio associated with incompressible behavior is .5) [14]. Therefore we have $-\mu\varepsilon = -\nu\varepsilon^{el} - .5\varepsilon^{in}$. Similarly, the lateral strain rate is $-\rho\dot{\varepsilon} = -\nu\dot{\varepsilon}^{el} - .5\dot{\varepsilon}^{in}$. Using these relations one can deduce that μ and ρ are both variable and different from one another in the following manner:

$$\mu = \frac{1}{2} - \frac{1}{E}\left[\frac{1}{2} - \nu\right]\frac{\sigma}{\varepsilon}$$

$$\rho = \frac{1}{2} - \frac{1}{E}\left[\frac{1}{2} - \nu\right]\frac{d\sigma}{d\varepsilon}$$

If the behavior is only a small departure from elasticity then $\mu \approx \rho \approx \nu$; conversely if a condition of strain and strain rate exists where inelastic behavior dominates and where $\sigma/\varepsilon \ll E$ and $d\sigma/d\varepsilon \ll E$ then the response is essentially incompressible with $\mu \approx \rho \approx .5$.

For the state of shear loading (superscript s) we have:

$$\varepsilon_{ij}^{s} = \begin{bmatrix} 0 & \frac{\gamma}{2} & 0 \\ \frac{\gamma}{2} & 0 & 0 \\ 0 & 0 & 0 \end{bmatrix} \quad \dot{\varepsilon}_{ij}^{s} = \begin{bmatrix} 0 & \frac{\dot{\gamma}}{2} & 0 \\ \frac{\dot{\gamma}}{2} & 0 & 0 \\ 0 & 0 & 0 \end{bmatrix} \quad \sigma_{ij}^{s} = \begin{bmatrix} 0 & \tau & 0 \\ \tau & 0 & 0 \\ 0 & 0 & 0 \end{bmatrix} \quad \beta_{ij}^{s} = \begin{bmatrix} 0 & \xi & 0 \\ \xi & 0 & 0 \\ 0 & 0 & 0 \end{bmatrix}$$

Here γ and $\dot{\gamma}$ are the engineering shear strain and strain rate, τ is the shear stress, and ξ is the shear backstress in the xy plane of Cartesian space.

By using the appropriate stress, backstress, and strain tensors, as well as their respective deviators and associated invariants, Eqs. (1)-(4) produce the following uniaxial equations:

$$\dot{\sigma} = E\left[\dot{\varepsilon} - \frac{2(1+\rho)}{3}|\dot{\varepsilon}|\left|\frac{\sigma-\beta}{Y}\right|^{n-1}\left[\frac{\sigma-\beta}{Y}\right]\{u(\varepsilon_0 - |\varepsilon|)\}\right]$$

$$\beta = E\alpha\left[\varepsilon - \frac{\sigma}{E} + f_T\,\mathrm{erf}\left[\frac{2(1+\mu)}{3}a\varepsilon\right]\{u(-\varepsilon\dot{\varepsilon})\}\right]$$

Note that ε_0 is the limiting strain for inelastic growth. At strains above ε_0 the damping mechanism is saturated and elastic behavior prevails. Also, $|\varepsilon|$ is the absolute value of ε. These equations can be further simplified by taking the total material response to be incompressible in the inelastic region (i.e. when $Y/E \le \varepsilon \le \varepsilon_0$). This simplification does not greatly affect the overall dissipative character of the axial response. Thus by setting $\mu = \rho = .5$ in the nonlinear inelastic response terms we obtain:

$$\dot{\sigma} = E\left[\dot{\varepsilon} - |\dot{\varepsilon}|\left|\frac{\sigma-\beta}{Y}\right|^{n-1}\left[\frac{\sigma-\beta}{Y}\right]\{u(\varepsilon_0 - |\varepsilon|)\}\right] \tag{5}$$

$$\beta = E\alpha\left[\varepsilon - \frac{\sigma}{E} + f_T\,\mathrm{erf}(a\varepsilon)\{u(-\varepsilon\dot{\varepsilon})\}\right] \tag{6}$$

Following the same process, the shear equations are:

$$\dot{\tau} = G\left[\dot{\gamma} - |\dot{\gamma}|\left|\frac{\tau - \xi}{Y_s}\right|^{n-1}\left(\frac{\tau - \xi}{Y_s}\right)\{u(\gamma_0 - |\gamma|)\}\right] \tag{7}$$

$$\dot{\xi} = \frac{E\alpha}{3}\left[\dot{\gamma} - \frac{\dot{\tau}}{G} + \sqrt{3}\, f_T\, \mathrm{erf}\left[\frac{a\gamma}{\sqrt{3}}\right]\{u(-\gamma\dot{\gamma})\}\right] \tag{8}$$

where

$\gamma_0 = \frac{2(1+\nu)}{\sqrt{3}}\varepsilon_0$ is strain limiting inelastic growth in shear

$G = \frac{E}{2(1+\nu)}$ is the elastic shear modulus

$Y_s = \frac{Y}{\sqrt{3}}$ is the shear stress whereupon the damping mechanism is activated

Note that Y_s falls out of the formulation automatically in a manner that is consistent with the theory of maximum distortional strain energy [15]. This is because Eq. (3) is dependent on the stress gradient of a potential function [13] that contains a von Mises type condition for the onset of the inelastic damping mechanism. Later the cases of bending and torsion will be modeled using finite difference geometries in conjunction with the above equations.

Now let us examine the results produced by numerical integration of Eqs. (5)-(6) and (7)-(8); a sinusoidal history of strain input was specified with strain amplitudes of ε_p in the axial case and γ_p in the shear case. These amplitudes were specified to be greater than the limiting strains so that the full character of the predicted response could be displayed in illustrative plots. The results of calculations for the axial and shear loading conditions are given in Figs. 4 and 5 respectively. Both figures possess the same characteristics: elastic behavior dominates in the region of the origin as well as outside the limiting strain, and a hysteresis loop is manifested in the full cycle of strain application. The area enclosed by the hysteresis loop represents the energy absorbed by the material undergoing cyclic oscillation. The elastic modulus of $E = 28.5 \times 10^6$ psi and limiting strain of $\varepsilon_0 = .0001$ were selected based on the elastic modulus and approximate strain of peak damping in Fe-Cr alloys (see Fig. 1). The remaining material constants used in the calculations that generated Figs. 4 and 5 were not selected to reproduce the behavior of any specified damping material; rather they were selected to approximate the general character of a nonlinear damping metal and allow for some investigative analyses. It should be noted that the results generated by the constitutive equations are numerically stable and insensitive to the rate of strain input [13]. Also the elastic and inelastic material properties (i.e. E, E_y, and Y) are accurately reproduced in numerical calculations [13].

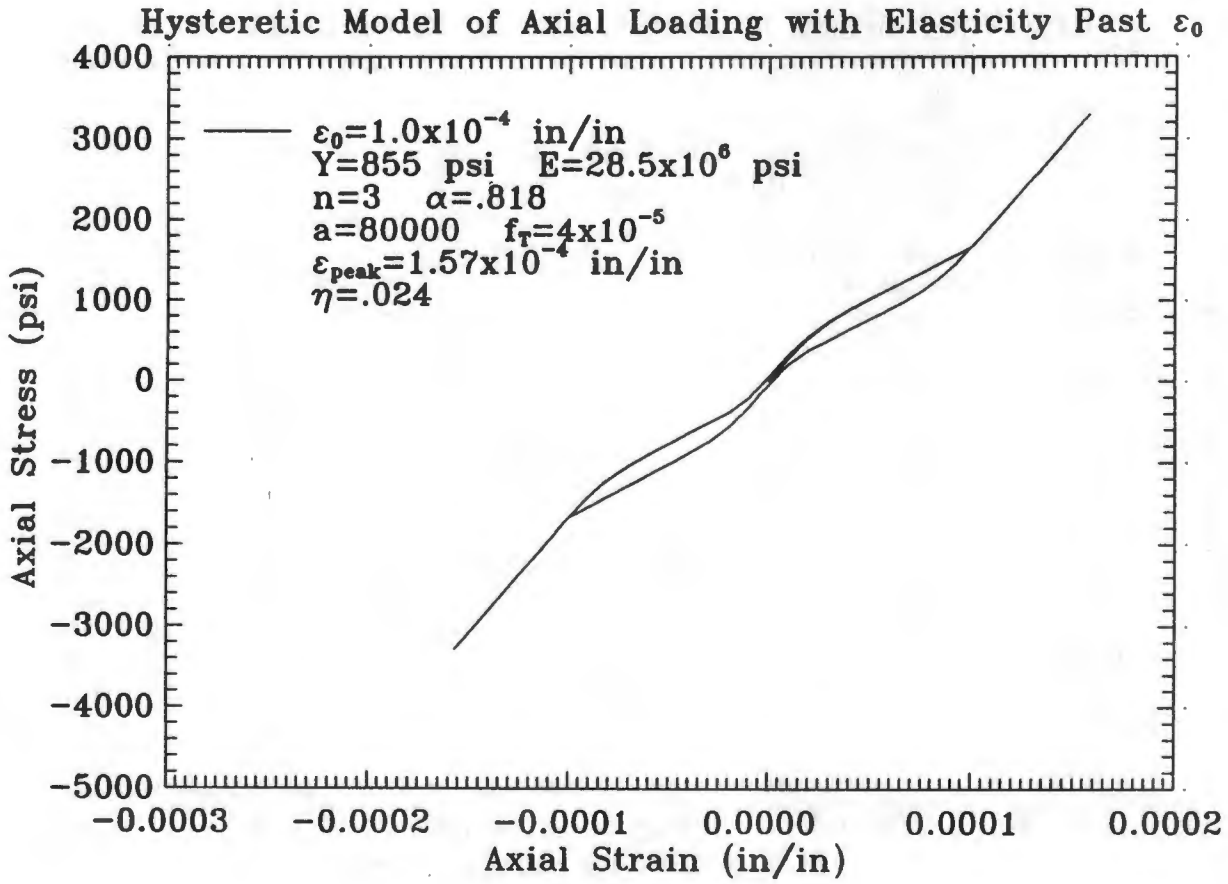

Figure 4: Hysteretic Behavior Calculated for Pure Axial Loading

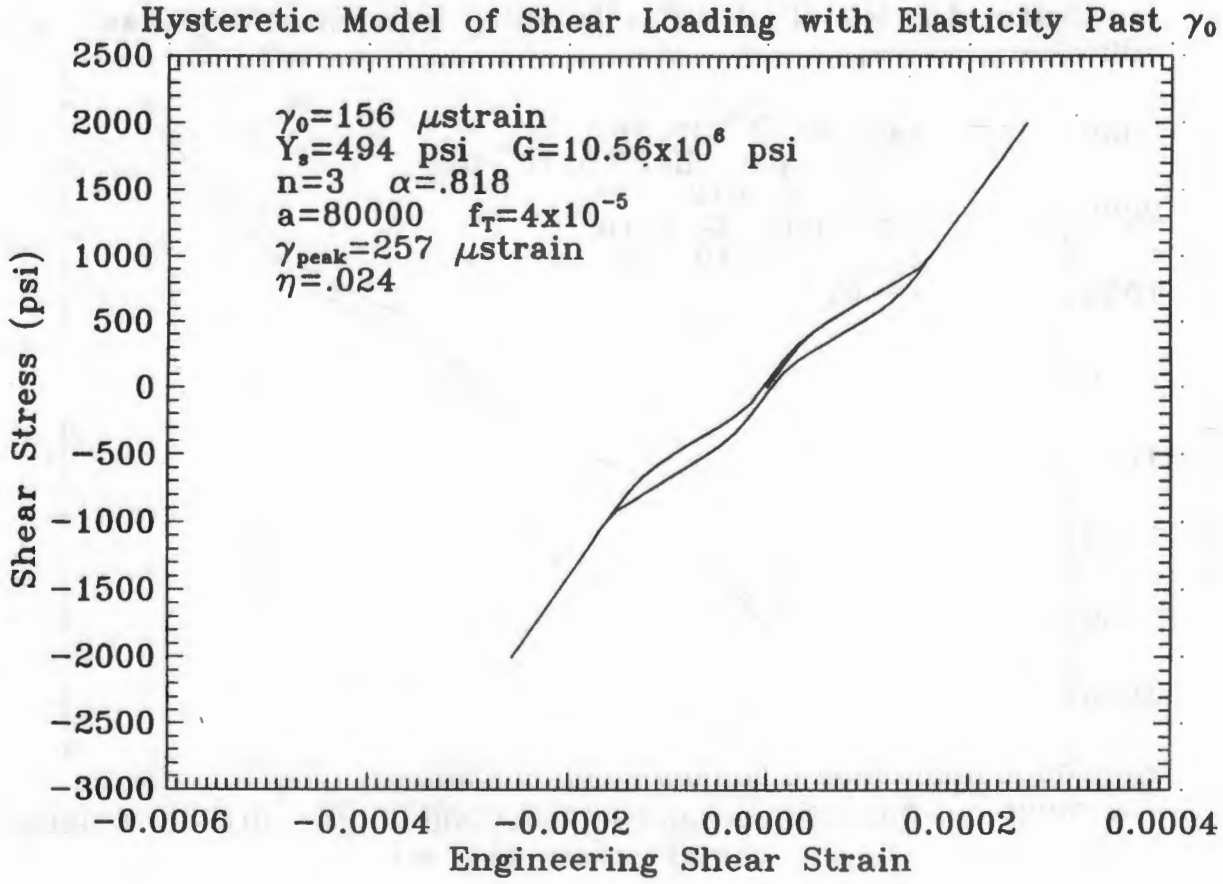

Figure 5: Hysteretic Behavior Calculated for Pure Shear Loading

By having numerical results of the type just presented, it is possible to numerically calculate the energy absorbed per cycle. We can then compute the material damping by dividing this energy by the product of 2π and an energy storage term. This corresponds to the measure of damping known as the loss factor η

$$\eta = \frac{\Delta W}{2\pi W} \tag{9}$$

In Eq. (9) ΔW is the energy absorbed due to damping and W is a measure of stored energy, often selected as

$$W = \frac{1}{2}\varepsilon_{max}\,\sigma\Big|_{\varepsilon_{max}} \tag{10}$$

When the damping mechanism is linear rather than nonlinear W represents the energy stored in a linear elastic material at peak strain. Also, for linear materials the loss factor is constant over a wide range strain because ΔW and W are proportional to one another. This is not the case for nonlinear materials. By using Eqs. (5)-(6) and (7)-(8) in calculations for the cyclic material response over a range of peak axial and shear strains, and computing the loss factor associated with each peak strain according to Eqs. (9) and (10), the general character of the damping vs. strain diagram of nonlinear materials was produced; this is shown in Fig. 6. Note that both curves possess the characteristic damping peak associated with nonlinear damping materials.

However the separate curves in Fig. 6 that represent axial and shear loading differ significantly with respect to one another. The cause of this difference was first investigated by evaluating the amount of energy absorbed in each loading configuration. The amount of energy absorbed, plotted as a function of peak strain, is given in Fig. 7. Above the respective limiting axial and shear strains the amount of energy absorbed by the material is essentially the same for both loading configurations, their difference being less than 1%. Therefore the difference in the character of the two separate responses must be due to other factors.

It turns out that the plots given in both Figs. 6 and 7 are misleading because the abscissa of these figures represents values of strain associated with separate axial and shear loading conditions, and the strains associated with these separate conditions are not equivalent. Therefore another measure of deformation equivalent to both types of loading needs to be employed. One such possibility is to use a measure of local distortion experienced by the strained material. Let us define an equivalent strain $\bar{\varepsilon}$ as follows:

$$\bar{\varepsilon} = \sqrt{3I_2} \tag{11}$$

This measure is similar to the effective plastic strain in plastically deforming materials [14]. It is clear that $\bar{\varepsilon}$ has a physical meaning that is independent of the choice of coordinate axes since it is based on the invariant I_2, which is the I_2 is the second invariant of the deviatoric strain e_{ij} (also

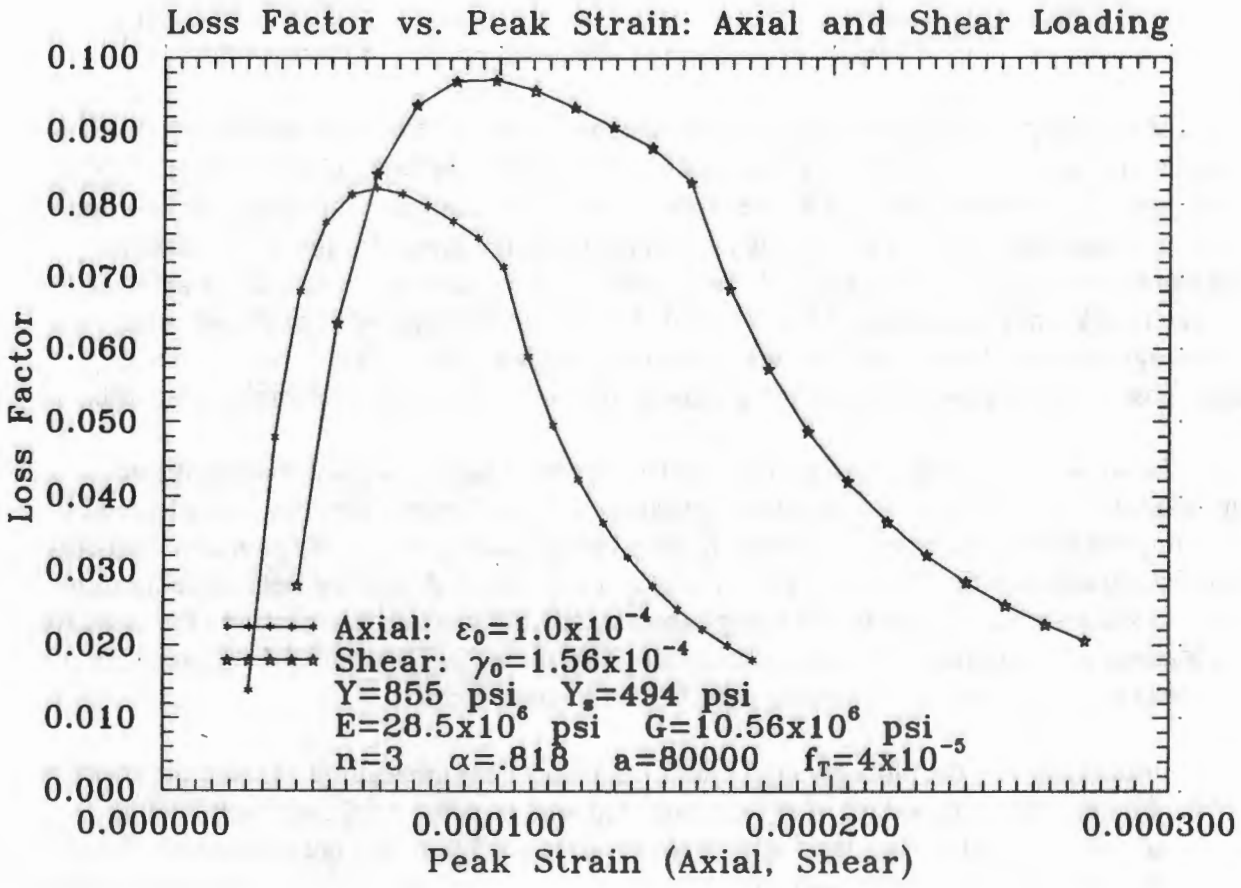

Figure 6: Strain Amplitude Depending Damping for Pure Axial and Shear Loading

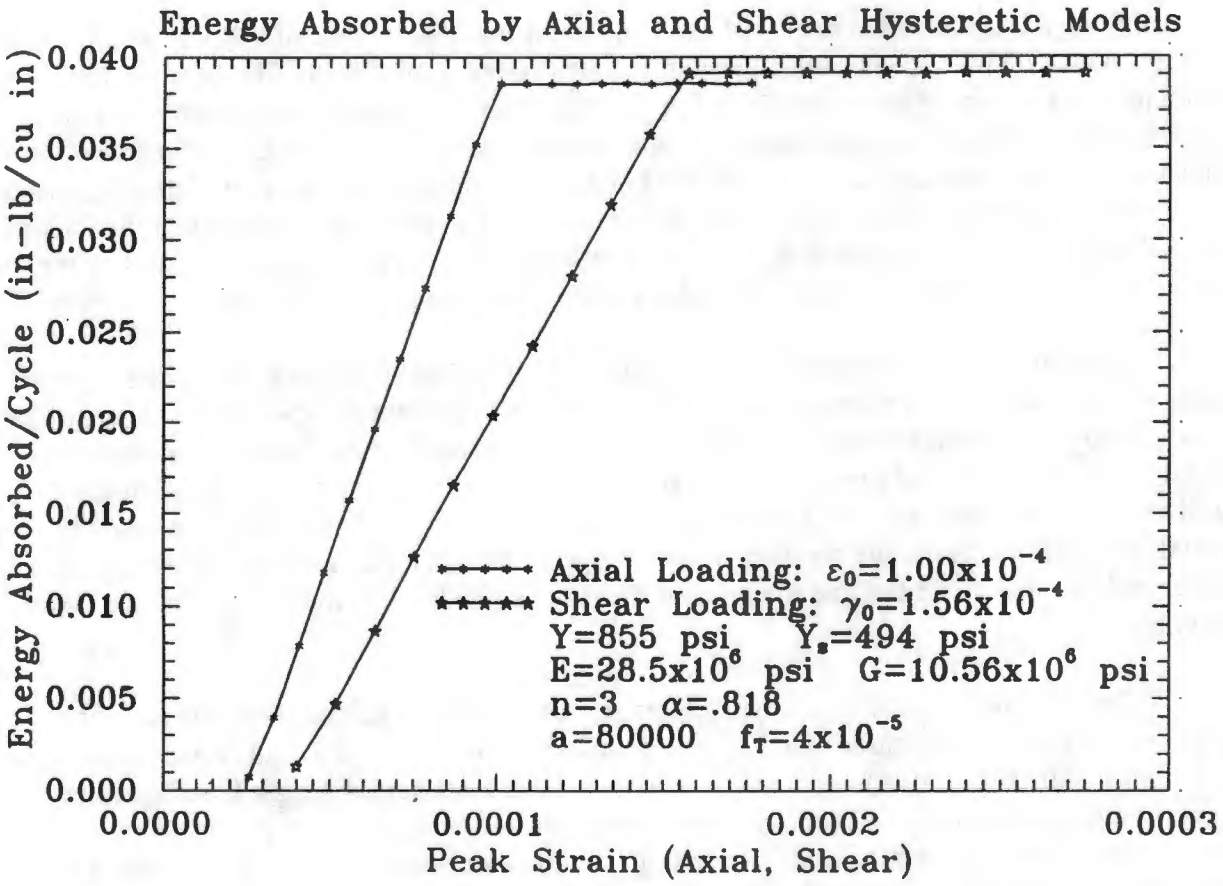

Figure 7: Energy Absorbed in Axial and Shear vs. Peak Axial and Shear Strains

called the distortional component of strain[3]). Therefore $\bar{\varepsilon}$ is an invariant measure of the local distortion.

By considering the separate states of axial and shear strain, and by taking the Poisson ratio to be the simple constant ν for axial case, one deduces that the equivalent strains for each state of strain are as follows:

$$\bar{\varepsilon}^{u} = (1 + \nu)\,\varepsilon \qquad \text{(uniaxial loading)}$$

$$\bar{\varepsilon}^{s} = \frac{\sqrt{3}}{2}\gamma \qquad \text{(shear loading)}$$

By using the peak equivalent strains of axial and shear loading in place of the peak strains used in Figs. 6 and 7 a more consistent pattern of results is developed. This is first done for the amount of energy absorbed as shown in Fig. 8. Note from this figure that for both cases the energy absorbed as a function of the distortion is in very good agreement along the entire abscissa. In Fig. 9 the loss factors of the axial and shear loading cases are also plotted against the peak equivalent strain. The results in this figure are now also much more consistent than before; indeed the breadth of each damping curve spans the same values of equivalent strain and the peak of each damping curve occurs at approximately the same level of distortion.

The only inconsistency that now remains is in the value of the peak loss factor of each separate curve and this is simply due to the occurrence of different values of stored energy being produced by the separate loading conditions. Indeed, because the modulus of the material in shear is lower than that of the same material under axial loading, the value of peak shear stress will also be lower than the peak axial stress at equivalent levels of distortion. Consequently, at equal levels of distortion, the measure of stored energy W will be larger in axial loading than in shear and this will cause the loss modulus in shear to be greater than the loss modulus in axial loading.

Because bending and torsion are common damping test configurations lets us next proceed to the following cases: bending of a solid beam having length L and rectangular cross-section of width b and thickness h, and torsion of a solid shaft having length L and circular cross-section of radius R. Even though the stress-strain response is nonlinear we can consider both cases in a simple fashion without needing to consider residual stresses or movement of the neutral axis of the beam. This is because the response takes place in a manner which gives symmetric behavior for positive and negative strains, and the response is hysteretic with essentially no residual strain. When considering bending and torsion problems with more pronounced inelastic behavior and residual stresses then special considerations must be made when computing the acting moments [16].

---

[3] The tensor e_{ij} is known as the distortional component of strain because, by definition, it subtracts the dilitational component of deformation out of the strain tensor ε_{ij}.

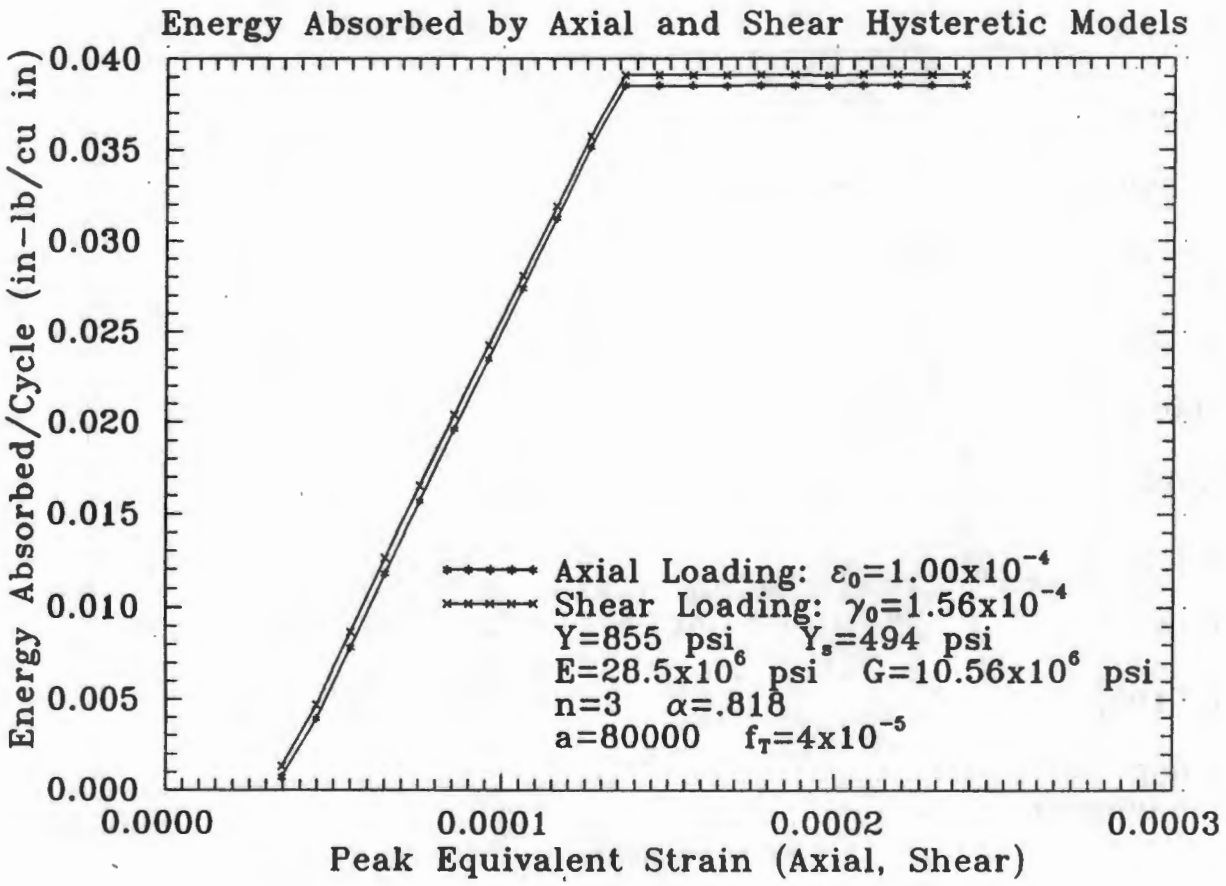

Figure 8: Energy Absorbed in Axial and Shear vs. Peak Equivalent Strain

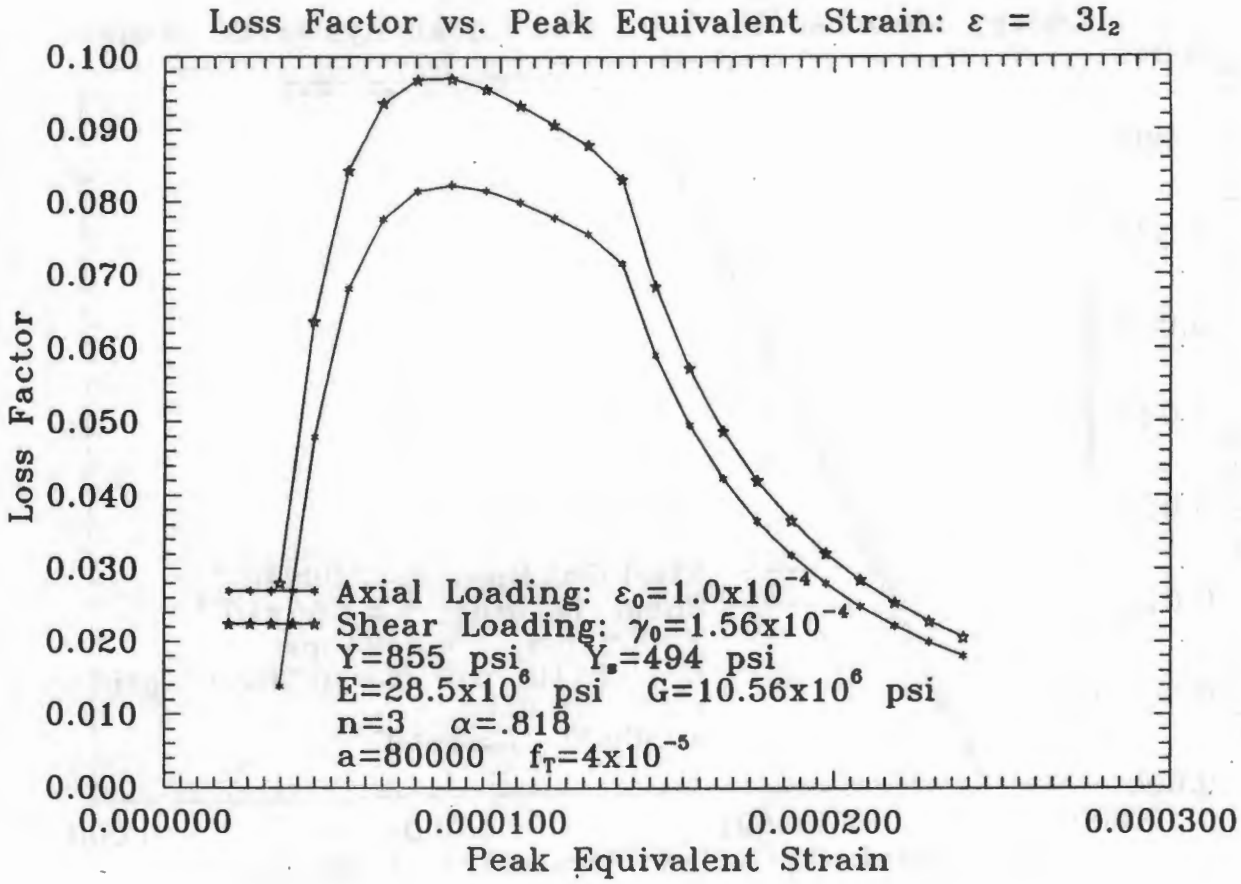

Figure 9: Amplitude Dependent Damping in Axial and Shear vs. Peak Equivalent Strain

Schematic illustrations of the bending and torsion cases are shown in Fig. 10. Note that the strain profiles in each geometry are linear, passing through zero at the position of the neutral axis of the beam and starting at zero at the center of the shaft. Also note that ε_p is the value of the axial strain at the beam surface while γ_p is the value of the engineering shear strain at the shaft surface. Because the problems under consideration involve only small strain, the following simple relations can be used to compute the moments and angular displacements for the beam and shaft geometries respectively:

$$M = -\int_A y\,\sigma\,dA \qquad \text{and} \qquad \theta = \frac{\varepsilon_p L}{h} \qquad \text{(beam)}$$

$$T = \int_A r\,\tau\,dA \qquad \text{and} \qquad \phi = \frac{\gamma_p L}{R} \qquad \text{(shaft)}$$

Here y is the vertical distance from the neutral axis of the beam cross-section, σ is the axial stress in the longitudinal fibers of the beam, M is the resultant moment bending the beam, and θ is the beam rotation; for the shaft r is the distance from the center of the circular cross-section, τ is the shear stress due to torsion, T is the resultant torque twisting the shaft, and ϕ is the angle of twist. In both cases A denotes the area of cross-section.

In analyses the surface strains of each geometry were specified to act sinusoidally in time. In addition each geometry was subdivided into a large number of finite, but thin, subsections; i.e. the infinitesimal distances dy and dr in Fig. 10 were replaced by small but finite distance Δy and Δr respectively. Also, the strain distribution for each finite subsection was assumed to be constant over the subsection thickness and the value of the strain was taken as the value of the strain profile at the center of the subsection. Having knowledge of the strain profile of the cross-section of each geometry, specifying the surface amplitudes and a sinusoidal history for each one, the stress history for each subsection of the geometry was computed numerically. Specifically, Eqs. (5)-(6) were integrated to give the stress profile time history of the bending beam and (7)-(8) were integrated for the shear stress profile time history of the shaft. Then the following formulas were used to compute the resultant moment and torque histories of the beam and shaft respectively:

$$M = -b \sum_{i=1}^{N} y_i\,\sigma_i\,\Delta y$$

$$T = 2\pi \sum_{i=1}^{N} (r_i)^2\,\tau_i\,\Delta r$$

where N is the number of subdivisions making up the cross-sectional geometry and where the subscript i indicates reference to the location of a single subsection.

Bending Beam (Length: L, Width: b, Thickness: h)

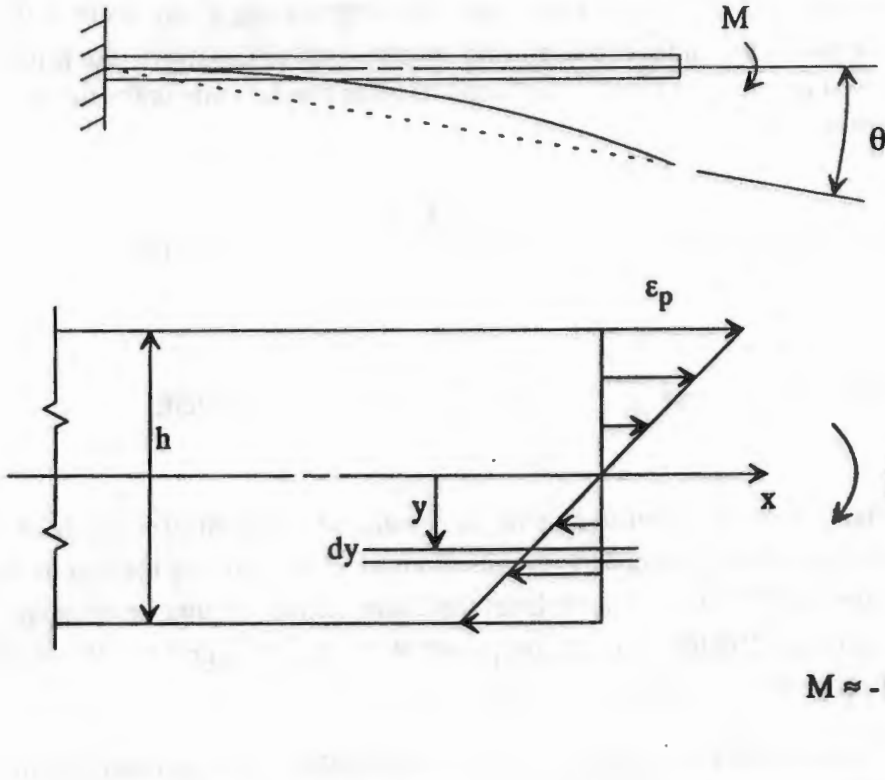

Twisting Shaft (Length: L, Radius R)

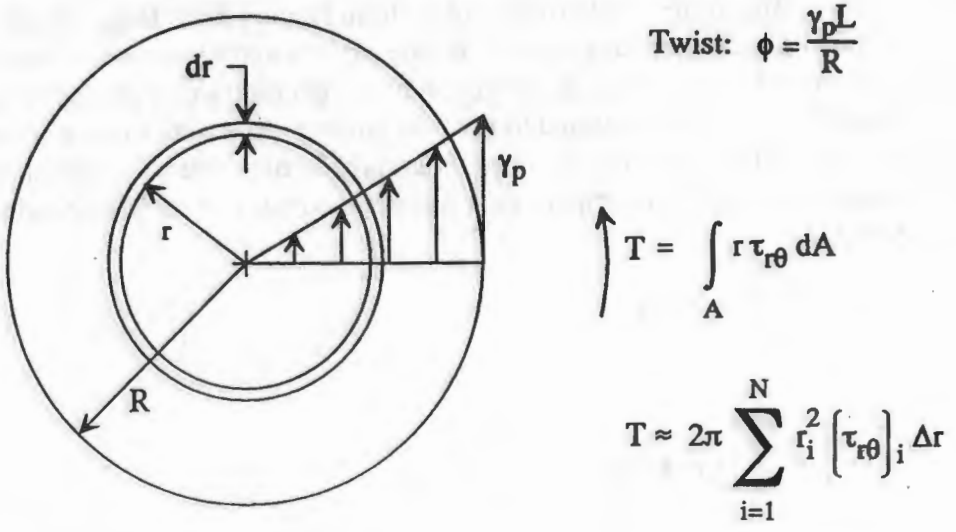

Figure 10: Schematic Drawing of Strain Profile in Bending and Torsion Geometries

The loss factor of each sample geometry was then calculated for a specified value of surface strain amplitude according to Eq. (9) where ΔW was determined by the area enclosed by the resultant moment vs. angular displacement hysteretic response and W was determined by

$$W = \frac{1}{2}\theta_{max} M\Big|_{\theta_{max}} \qquad \text{(beam)}$$

$$W = \frac{1}{2}\phi_{max} T\Big|_{\phi_{max}} \qquad \text{(shaft)}$$

The damping values which were computed in this way were found to be independent of sample geometry, i.e. for a given surface amplitude the ratio of ΔW to W remained constant for changes in cross-sectional size, sample length or both.

By repeating the calculations over a range of surface amplitudes the loss factor was plotted against the surface amplitude for both the bending and torsion cases as shown in Fig. 11. Note that the character of the damping vs. surface amplitude curves are vastly different with respect to one another. This is analogous the trend shown earlier in Fig. 6 for one dimensional behavior. Also, by comparing Fig. 11 to Fig. 6 it is clear that the character of the damping vs. peak strain curve of each sample is quite different than that corresponding to the respective one-dimensional material point responses. This is because of the strain dependent nature of the damping and the fact that strain is distributed throughout the sample; therefore some regions of the geometry may be contributing significantly to the overall damping of the solid sample while others are not.

As was done earlier, the inconsistent nature of the results given in Fig. 11 can be improved by making use of the peak equivalent strain $\bar{\varepsilon}$ at the surface rather than the surface strain amplitude alone. Using Eq. (11) to calculate the amounts of peak equivalent strain at the surface of the bending and torsion samples, and plotting the corresponding loss factors of each sample against these values produces the curves given in Fig. 12. This figure shows that the use of peak equivalent strain for the finite sized geometries of bending and torsion samples gives an improved measure of correlation in the same manner that was exhibited earlier for the one-dimensional cases.

Thus presentation of nonlinear damping data as a function of equivalent strain rather than as a function of sample strain can be very useful. It is probably most useful in comparing damping data obtained by different test methods. It may also be useful in design work where the dynamic strains in a vibrating part or member are known. To show this let us consider an example where a designer wishes to use a high damping, but nonlinear, material in an application where bending is the primary mode of deformation, and suppose that damping data is available only from torsional tests. If the vibrational strain levels to be expected in service can be deduced from load and design analyses, then these strain levels can be converted to the measure of equivalent strain introduced in this paper. Applying the same conversion to the peak shear

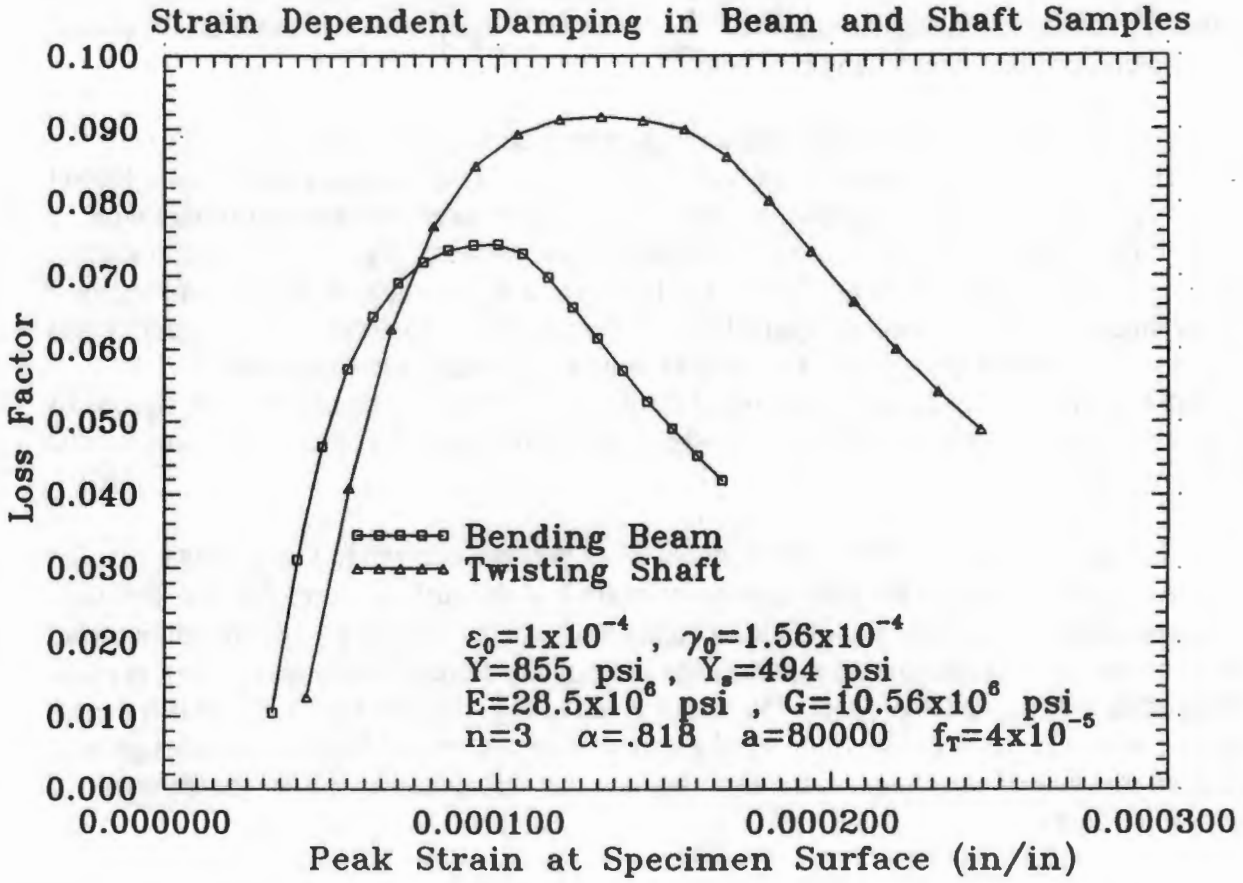

Figure 11: Amplitude Dependent Damping in Bending and Torsion vs. Peak Surface Strain

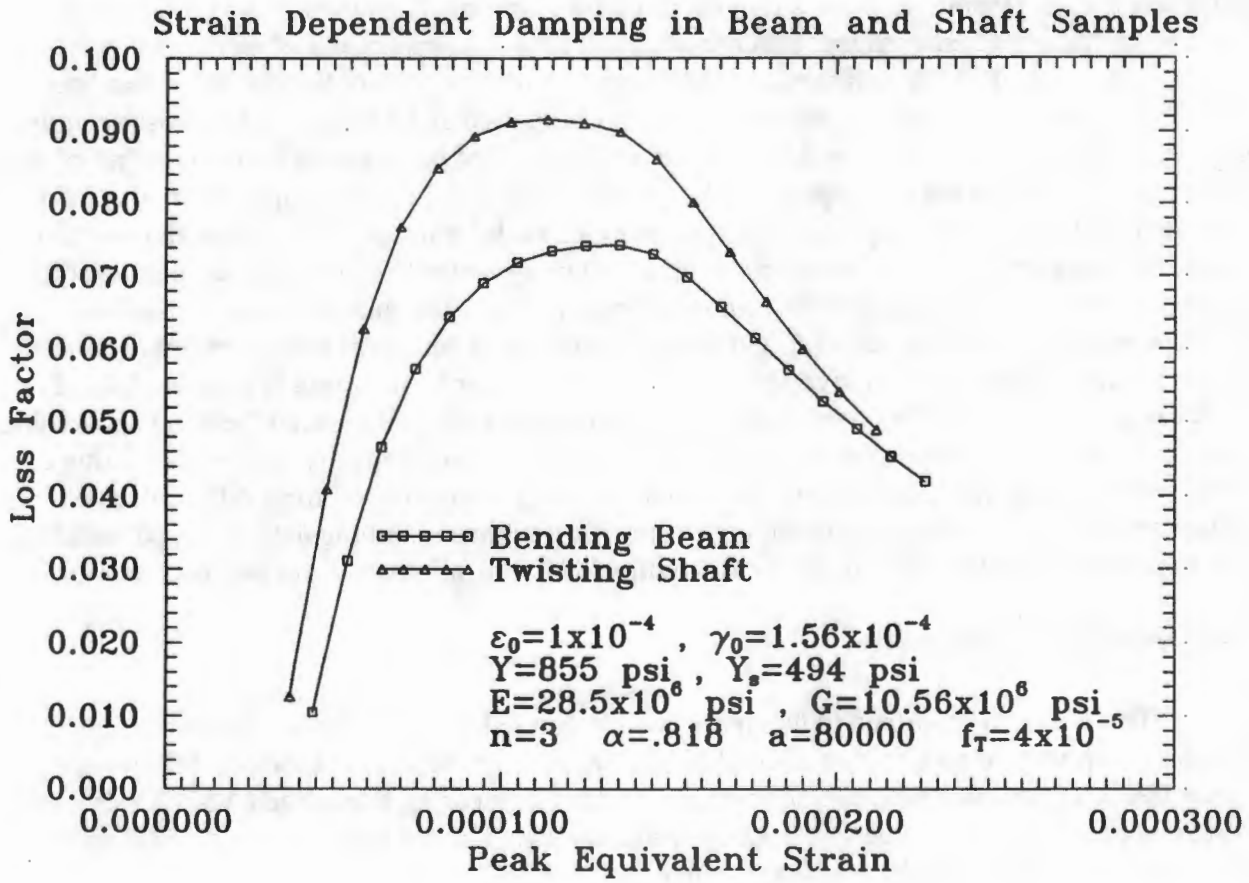

Figure 12: Amplitude Dependent Damping in Bending and Torsion vs. Peak Equivalent Strain

strains of the torsional damping data the designer would then be able to estimate whether or not the material damping will be in a range of peak performance for the application of interest.

SUMMARY

The work presented in this paper includes two major aspects; 1) modeling of nonlinear (or strain dependent) damping behavior via constitutive equations and 2) a way of improving correlation of nonlinear damping data via use of equivalent measures of distortion. These efforts were conducted in order to gain a better understanding of macroscopic nonlinear high damping material behavior and also to obtain a means in which to better correlate existing discrepancies in reported data for high damping materials. The modeling scheme applies to homogeneous isotropic materials and is adapted from a viscoplastic law through incorporation of material constants that correspond to small strain damping mechanisms. Also the law was modified to include damping mechanisms that become saturated after a given amount of strain. Analyses were made to calculate the loss factor of the common damping test configurations of bending and torsion. To do this material point relationships were used at each point in the cross-sectional geometry. In this way it was possible to relate the damping of the material to the damping of the specimen. The results did not depend on the relative dimensions of the sample geometry; rather the calculated loss factors depended only on the mode of deformation. The results showed that the strain dependent damping associated with each test were vastly different when plotted solely against the peak surface strain of the sample geometry. This is because the peak strains that correspond to each of these test configurations, namely axial and shear strain, are not equivalent to one another. However if an invariant measure of peak sample distortion is used in place of peak sample strain, then the correlation of the nonlinear damping of separate bending and torsion samples is predicted to improve considerably. Such an improved capacity for the correlation of nonlinear damping data may be very useful in comparing data obtained from different tests. Future research will include the modeling of specific nonlinear damping data. Also, constitutive law material parameters that are physically motivated by the microstructure will be studied.

ACKNOWLEDGEMENT

This research described in this paper was performed at David Taylor Research Center, and was supported in part by an Office of Naval Technology (ONT) postdoctoral fellowship under the administration of the American Society for Engineering Education (ASEE). Also, the research was supported by the Quiet Alloys Program which is part of the Functional Materials Block Program sponsored by Mr. Ivan Caplan.

REFERENCES

1. Perkins, A.J., Edwards, G.R., and Hills, N.A., "Materials Approaches to Ship Silencing," Report No. NPS-59Ps74061, Naval Postgraduate School, Monterey, California, June, 1974.

2. Schetky, L.M. and Perkins, J., "The 'Quiet' Alloys," *Machine Design*, April 6, 1978, pp. 202-206.

3. Dew, D., "Strain Dependent Damping Characteristics of a High Damping Manganese-Copper Alloy," Report No. NPS69-86-007, Naval Postgraduate School, Monterey, California, September, 1986.

4. Suzuki, K., Fujita, T., and Hasebe, M., "Damping Capacity and Mechanical Properties of Sintered Fe-Cr-Mo High Damping Alloys," *Proceedings of the 6th International Conference on Internal Friction and Ultrasonic Attenuation in Solids*, Hasiguti, R. and Mikoshiba, N. (ed.), University of Tokyo Press, 1977, pp. 757-761.

5. Schneider, W., Schrey, P., Hausch, G., and Török, E. "Damping Capacity of Fe-Cr and Fe-Cr Based High Damping Alloys," *Journal De Physique*, Colloque C5, Supplément au n° 10, Tome 42, October, 1981, pp. C5-635 - C5-639.

6. Masumoto, M., Hinai, M., and Sawaya, S., "Damping Capacity and Pitting Corrosion Resistance of Fe-Mo-Cr Alloys," *Transactions of the Japan Institute of Metals*, Vol. 25, No. 12, 1984, pp. 891-899.

7. Nippon Kokan K.K., Tranqaloy Data Sheets, 1981.

8. Kawabe, H. and Kuwahara, K., "A Consideration of the Strain Dependent Damping and Modulus in Ferromagnetic Metals," *Transactions of the Japan Institute of Metals*, Vol. 22, No. 5, 1981, pp. 301-308.

9. Lazan, B.J., "Effect of Damping Constants and Stress Distribution on the Resonance Response of Members," *Journal of Applied Mechanics*, Transactions of the ASME, Vol. 75, 1953, pp. 201-209.

10. Cochardt, A.W., "A Method for Determining the Internal Damping of Machine Members," *Journal of Applied Mechanics*, Transactions of the ASME, Vol. 76, 1954, pp. 257-262.

11. Krempl, E., "Models of Viscoplasticity: Some Comments on Equilibrium (Back) Stress and Drag Stress," *Acta Mechanica*, Vol. 69, 1987, pp. 25-42.

12. Miller, A.K. (ed.), *Unified Constitutive Equations for Creep and Plasticity*, Elsevier Applied Science, 1987.

13. Graesser E., "Multi-Dimensional Modeling of Hysteretic Materials Including Shape Memory Alloys: Theory and Experiment," Ph.D. Dissertation, Dept. of Mechanical and Aerospace Engineering, State University of New York at Buffalo, Buffalo, New York, February, 1990.

14. Shames, I.H. and Cozzarelli, F.A., *Elastic and Inelastic Stress Analysis*, Prentice-Hall, 1991.

15. Shames, I.H., *Introduction to Solid Mechanics*, Prentice-Hall, 1975.

16. Timoshenko, S.P. and Goodier, J.N., *Theory of Elasticity*, Third Edition, McGraw-Hill, 1970.